DOI: 10.1002/adfm.200600783

Soft Lithography of Ceramic Patterns**

By *Ole F. Göbel*, *Mihaela Nedelcu*, and *Ullrich Steiner**

Polymer-based precursor solutions are patterned using a soft-lithographic patterning technique to yield sub-micrometer-sized ceramic patterns. By using a polymer–metal-nitrate solution as a lithographic resist, we demonstrate a micromolding procedure using a simple rubber stamp that yields a patterned precursor layer. A subsequent high-temperature annealing step degrades the polymer giving rise to a patterned metal oxide film. This procedure is demonstrated for three different ceramic materials: Al_2O_3, ZnO, and $PbTiO_3$. Al_2O_3 initially forms an amorphous phase that is subsequently converted into a polycrystalline material upon electron irradiation. The formed ZnO and $PbTiO_3$ are polycrystalline. $PbTiO_3$ exhibits epitaxial alignment when cast onto a $SrTiO_3(001)$ surface that matches its lattice periodicity. This epitaxial alignment is maintained when the $PbTiO_3$ phase is patterned by micromolding, giving rise to epitaxially grown $PbTiO_3$ patterns with feature sizes down to 300 nm.

1. Introduction

Soft lithography is an increasingly important technology for low-cost pattern replication with implications for a wide variety of applications.[1] Making use of rubber stamps, soft-lithographic methods involve the transfer of the relief pattern of a stamp into a self-assembled monolayer (microcontact printing), or into a thin film that typically consists of an organic material (micromolding). These techniques developed by Whitesides and co-workers in the 1990s have spawned a large number of related methods.[1] The common denominator of nearly all soft-lithographic methods is that they are typically best suited for patterning "soft" materials, such as polymers, short end-functionalized organic chains, and biological macromolecules.

Less well studied are the liquid-deposition methods used to manufacture thin patterned layers and their combination with soft lithography. Micromolding in capillaries has been used to pattern ionic salts and glasses employing low-temperature sol–gel reactions.[2] Using a combination of micromolding and self-assembly, micropatterned silica films have been obtained with a high degree of orientational order.[3] Using high-temperature pyrolysis, a number of different ceramic materials have been patterned at micrometer and sub-micrometer length scales.[4] Over the last decade, this work has been extended to a number of different systems.[5–13] The resulting patterned ceramics are typically amorphous or polycrystalline.

In addition to ceramic films that have no orientation with respect to the substrate, the growth of epitaxial films using liquid-deposition techniques is also possible.[14–17] An epitaxially aligned ceramic material has been patterned by a molding technique to create 50 μm wide lines;[18] however, epitaxially aligned structures with sub-micrometer resolution have not yet been demonstrated by using soft lithography. Such an extension of soft lithography is attractive because thin films with properties that rely on or benefit from epitaxial order (e.g., piezoelectric and high-T_C (Curie temperature) superconducting properties) can possibly be patterned with sub-micrometer-scale precision. In contrast to more-established deposition methods, liquid deposition is attractive, because, from the practical point of view, it is considerably simpler than the competing methods.

We show here that by using polymer-based precursors it is possible to pattern ceramic materials using soft lithography. It is not only possible to epitaxially grow thin ceramic films from organic solutions,[15–18] but also to pattern these films by a simple micromolding method. The application of soft lithography to epitaxially grown ceramic films is attractive, because it extends this technique towards functionalities that cannot be achieved by using amorphous or polycrystalline materials. The possibility of obtaining epitaxially aligned materials that are patterned with sub-micrometer-scale precision offers many interesting opportunities. We demonstrate here the fabrication of an array of epitaxial material with a sub-micrometer lateral pattern size. The generic nature of this experimental technique allows the extension of this method to a large class of ceramic materials.

---

[*] Prof. U. Steiner, M. Nedelcu
Department of Physics, Cavendish Laboratory
University of Cambridge
J. J. Thomson Avenue, Cambridge CB3 0HE (UK)
E-mail: u.steiner@bss.phy.cam.ac.uk
Prof. U. Steiner, M. Nedelcu
The Nanoscience Center, Interdisciplinary Research Collaboration in Nanotechnology
University of Cambridge
11 J. J. Thomson Avenue, Cambridge CB3 0FF (UK)
Dr. O. F. Göbel,[+]
Department of Polymer Chemistry and Materials Science Center
University of Groningen Nijenborgh 4
9747 AG Groningen (The Netherlands)

[+] Present address: Faculty of Science and Technology, University of Twente, P.O. Box 217, 7500 AE Enschede, The Netherlands.

[**] We acknowledge the help of B. J. Kooi (TEM imaging), H. Nijland and M. Smithers (SEM imaging), and T. Hibma (use of X-ray diffractometer).

2. Results and Discussion

In the first set of experiments, polycrystalline films of simple oxides have been prepared. To demonstrate the versatility of our approach, two experimental systems were selected: Al_2O_3 and ZnO. Aluminium oxides are often used as dielectric insulators (they have dielectric constants as high as 7.7 and their resistivities can range up to 10^{16} Ω cm), and are also of interest because of their hardness. ZnO is a wide-bandgap semiconductor that can be doped to yield a transparent, highly conductive material.

Layers of both materials have been prepared in an analogous manner. The nitrate of the metal was dissolved in *N*,*N*-dimethylformamide (DMF), and poly(acrylic acid) (PAA) was added to the solution. The solution was then deposited onto an oxide-covered silicon wafer or a glass slide by spin-coating or micromolding, and the resulting film was subsequently dried. This caused the metal ions to be complexed by the polymer, leading to a homogeneous distribution of the metal ions in the polymer matrix. The films were then heated in two stages: first to 500 °C to degrade the polymer and to remove the degradation products, followed by an annealing step at a temperature of ca. 600 °C during which the oxide phase was formed. Figure 1a shows a spin-cast Al_2O_3 film after annealing. The film was very smooth with a surface roughness of less than 3 nm (Fig. 1b).

To investigate the thermodynamic phase of the film, electron diffraction patterns were acquired for films that were spin-cast onto microscope cover slips. Interestingly, after preparation, the Al_2O_3 was observed to be amorphous. The electron diffraction pattern shown in Figure 1c is characterized by a halo. Crystallization of the oxide phase can be induced through electron irradiation. Figure 1d shows the electron diffraction pattern after prolonged irradiation with 200 kV electrons. From the diffraction pattern, the Al_2O_3 phase was identified as either γ- or η-Al_2O_3. In contrast, ZnO formed a crystalline phase (zinkite) after annealing, as shown in Figure 2a. The relative peak heights of the X-ray diffraction pattern are indicative of the polycrystalline nature of the film.

The advantage of using polymer-containing precursor solutions is that their viscosity can be controlled by adjusting the polymer concentration and molecular weight. This enables the use of a number of soft-lithography methods. In this study, a micromolding process was used: a poly(dimethylsiloxane) (PDMS) rubber mold with micrometer-sized lateral surface topography was pressed into a few drops of the precursor solution and the assembly was heated to 80 °C for ca. 50 min to dry the film. After the removal of the mold, the samples were subjected to the heating protocol described above. Figure 2b and c shows an array of ZnO lines (ca. 180 nm in width) and Al_2O_3 columns (ca. 265 nm in diameter). The molds for both patterns had a lateral feature dimension of 800 nm. The 100 nm dimensions were therefore a consequence of the volume reduction during annealing. The lateral contraction of the columns by ca. 89 % was much larger compared to the stripes, whose width contracts by ca. 78 %. Assuming that the relief of the mold was fully filled by the precursor solution during micromolding, the stripes exhibit a higher degree of vertical shrinkage (ca. 93 %), compared to the columns (ca. 79 %). The apparent volume contraction of 98–99 % is larger than the predicted volume reduction of ca. 95 % calculated from the stoichiometry of the precursor solution. This discrepancy is probably due to incomplete filling of the mold during micromolding. These patterns were highly reproducible and nearly defect free over almost the entire sample area of 1 cm × 1 cm.

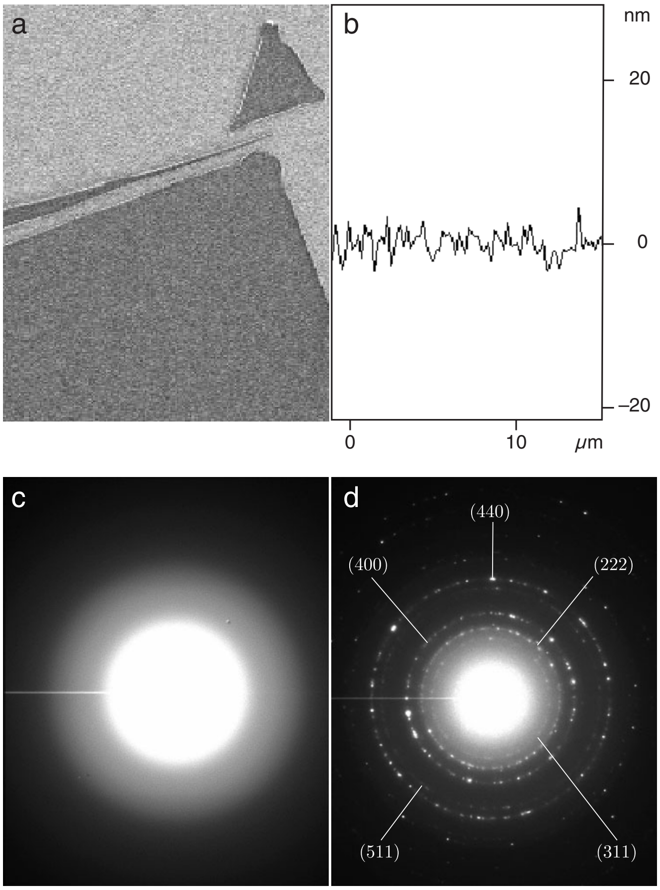

Figure 1. Al_2O_3 films on a microscope cover slip. a) The scanning electron microscopy image shows a fragment of the film. b) Cross section of the corresponding atomic force microscopy scan shows a root-mean-square roughness of 3 nm. The as-prepared Al_2O_3 films are amorphous. c) The transmission electron microscopy diffraction image shows a diffuse halo. Upon prolonged electron irradiation the diffraction image shown in (d) appears. The indexed diffraction rings can be ascribed to either γ- or η-Al_2O_3.

The second experimental series consisted of $PbTiO_3$ thin films grown on $SrTiO_3(001)$ single crystals and silicon wafers. $PbTiO_3$ is one end member of the solid solution series $PbZrO_3$–$PbTiO_3$ (PZT). Patterned PZT materials are of interest as micromechanical actuators and for ferroelectric data storage. As both the spontaneous and stress-induced polarization are parallel to the $\vec{c}$-axis, a preferential orientation of the $\vec{c}$-axis perpendicular to the plane of the film is desirable. The strongest effect can be obtained by epitaxial growth of the ferroelectric on a suitable substrate. The experimental system used is similar to the ones described above: nitrates of Pb and

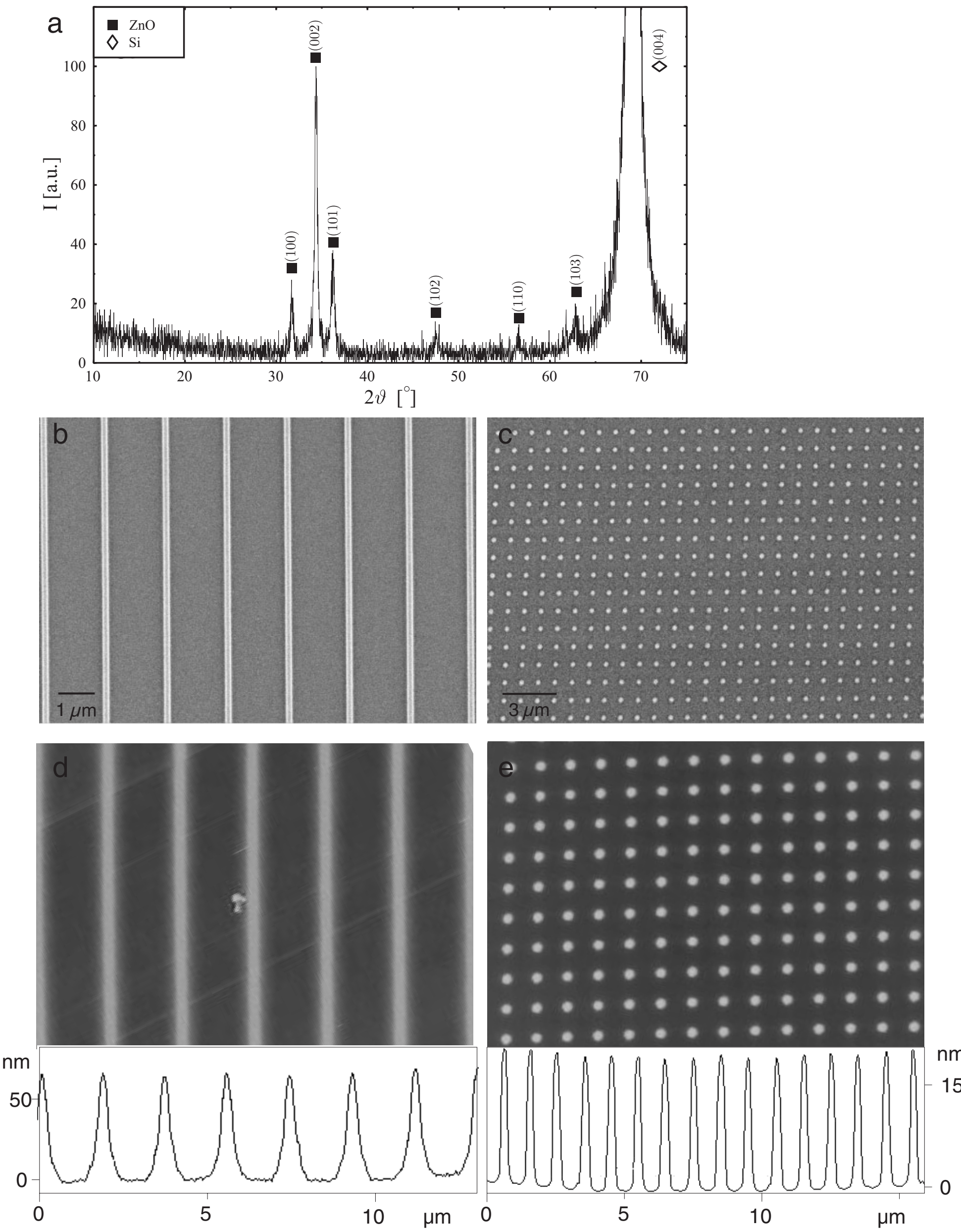

Figure 2. ZnO and Al_2O_3 films on a) a silicon wafer and b–e) microscope cover slips. All peaks in the ω–2θ scan of ZnO in (a) can be indexed to either ZnO or Si (for this and all other X-ray scans, cubic substrate lattices have been chosen such that the $\vec{c}$-axis of the substrate is parallel to the film normal). The scanning electron microscopy image of ZnO in (b) shows a film patterned by micromolding using a mold with a line width of 800 nm and a periodicity of 1.8 μm (the lines in (b) and (d) are doped with ca. 2 % Al). The Al_2O_3 dot array in (c) has been made with a mold that has 800 nm wide holes with a 1 μm periodicity. The corresponding atomic force microscopy images and cross sections are shown in (d) and (e). The lateral pattern sizes determined from (b) and (c) are ca. 180 and 265 nm, respectively. The pattern heights determined from (d) and (e) are ca. 65 and 200 nm, respectively.

Ti are dissolved in a 1:1 molar ratio in DMF and PAA is added. Films are prepared by spin-coating or micromolding and a two-step high-temperature heating protocol is used with a maximum temperature of 700 °C. In contrast to the amorphous film shown in Figure 1a, the surface of spin-cast and annealed $PbTiO_3$ films on $SrTiO_3(001)$ is not smooth, and is instead characterized by surface corrugation with height variations of several tens of nanometers (Fig. 3a). Careful examination of the surface morphology reveals the nature of this corrugation as arising from surface reconstruction that locally mirrors the symmetry of the underlying $SrTiO_3$ substrate. The epitaxial orientation of $PbTiO_3$ on $SrTiO_3$ is better shown by an ω–2θ X-ray scan. Figure 3b and d compares $PbTiO_3$ deposited on a silicon wafer (with a native oxide layer) and on a $SrTiO_3(001)$ single crystal. In the latter case only the $(00l)$ peaks of $SrTiO_3$ and the $(00l)$ peaks of $PbTiO_3$ are discernible, indicating the

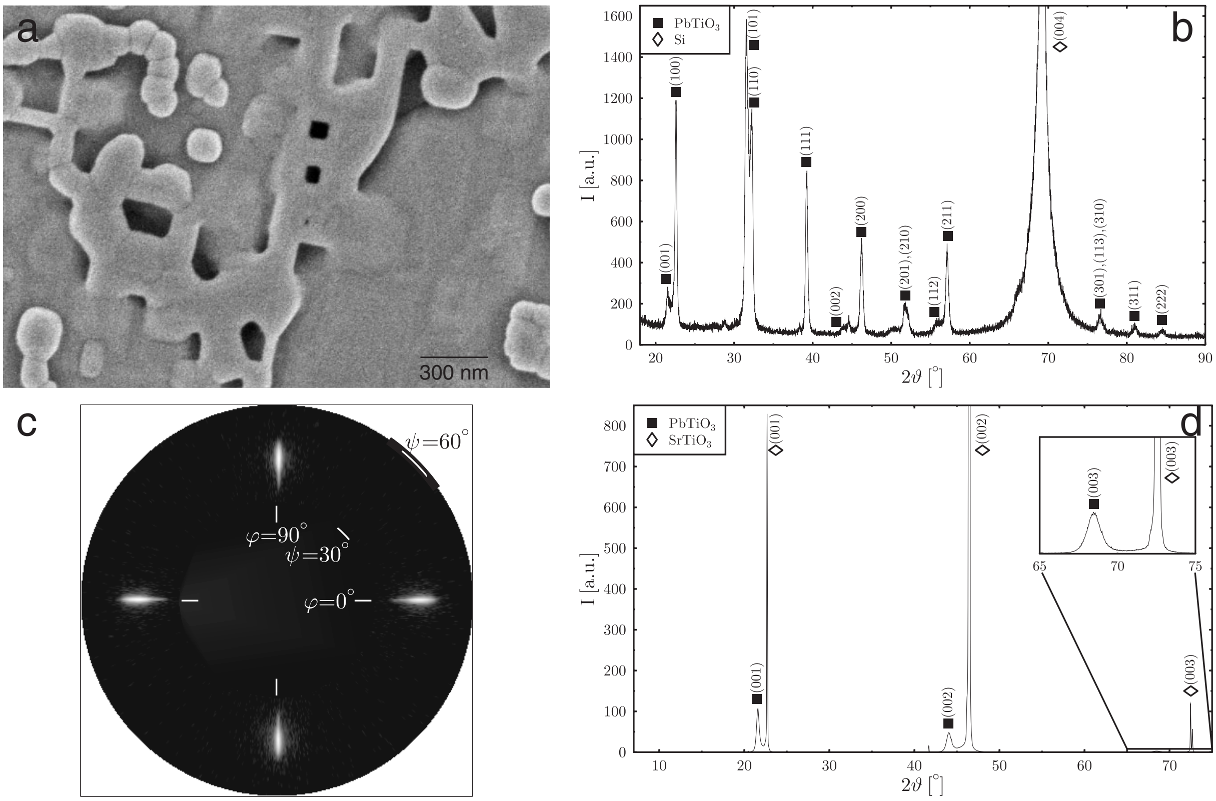

Figure 3. PbTiO$_3$ deposited on two different substrates. While PbTiO$_3$ forms a smooth film on Si wafers (not shown), on SrTiO$_3$(001) substrates, PbTiO$_3$ films show a characteristic terraced appearance. The ω–2θ scans in (b) and (d) show a comparison of PbTiO$_3$ on an oxide-covered Si(001) wafer and a SrTiO$_3$(001) surface, respectively. Whereas the scan in (b) resembles a PbTiO$_3$ powder diffractogram, only the (00*l*) peaks of PbTiO$_3$ and SrTiO$_3$ are visible in (d). Since the (00*l*) peaks of SrTiO$_3$ and the (*h*00) peaks of PbTiO$_3$ nearly coincide, no information about the amount of $\vec{a}$-oriented material can be obtained from (d). The four {101} peaks in (c) provide evidence for the epitaxial orientation of PbTiO$_3$ on SrTiO$_3$, which is either purely $\vec{c}$- or mixed $\vec{c}$- and $\vec{a}$-oriented. This diffraction image has been obtained by adjusting the diffraction set-up so that the PbTiO$_3$(101) peak is detected. Upon rotation of the sample around its normal, the detection of the {101} peaks at mutually orthogonal angles is evidence for the in-plane alignment of the PbTiO$_3$ film with respect to the underlying SrTiO$_3$ substrate. The radial coordinate in the polar plot corresponds to the variation of the tilt angle ψ during the scan.

$\vec{c}$-axis orientation of PbTiO$_3$ on SrTiO$_3$. In addition, the pole figure of the {101} reflections of PbTiO$_3$ in Figure 3c provides further proof of the in-plane orientation of PbTiO$_3$ and the epitaxial relationship between PbTiO$_3$ and SrTiO$_3$. We have recently presented similar results for the epitaxial growth of $Bi_2Sr_2CaCu_2O_x$ and $YBa_2Cu_3O_{7-\delta}$ high-T_C superconductors. The mechanism for the formation of epitaxial layers by a simple liquid deposition process has been explained by Seiffert et al.[14]

Analogous to the results presented in Figure 2, it is possible to generate thin patterned PbTiO$_3$ films on silicon wafers and SrTiO$_3$ surfaces by micromolding. The atomic force microscopy (AFM) images in Figure 4a and b show a similar quality of replication and similar lateral structure sizes—lines with a width of ca. 700 nm and columns with a width of ca. 1 µm on silicon wafers. The heights of the structures are 90 and 115 nm, respectively. As compared to the lateral pattern dimensions of the mold (1.2 µm (lines) and 1.4 µm (dots)), lateral shrinkages of 42 and 49 % are observed in Figure 4a and b, respectively. The vertical shrinkage in Figure 4a and b is 90 and 88 %, respectively, and the overall volume contraction is ca. 94 %, which is in good agreement with the predicted volume contraction of ca. 95 %.

In addition to the polycrystalline patterns shown in Figure 4a and b, the scanning electron microscopy (SEM) images in Figure 4c and d show the epitaxial alignment of a PbTiO$_3$ pattern on SrTiO$_3$(001). The quality of pattern replication can be more clearly observed in the corresponding AFM image in Figure 5. Due to the low overall surface coverage of the columns in the patterned films, the analysis of these features by X-ray diffraction is difficult. Instead, the morphological details of a single column are shown. Figure 4c shows the SEM image of a single column. In this sample, a thin, incomplete layer of PbTiO$_3$ surrounds the column. The holes in the layer have colinear straight edges parallel to the [100] and [010] edges of the SrTiO$_3$ substrate, indicating the epitaxial nature of this layer. Whereas the morphology of the PbTiO$_3$(001) columns is somewhat rounded, it is possible to identify faceted aspects of the columns. The faces of the column are also parallel to the edges of the substrate. A similar, somewhat larger column is shown in Figure 4d. The lines indicate the direction of the edges of the single-crystal SrTiO$_3$ substrate. While definitive evidence of

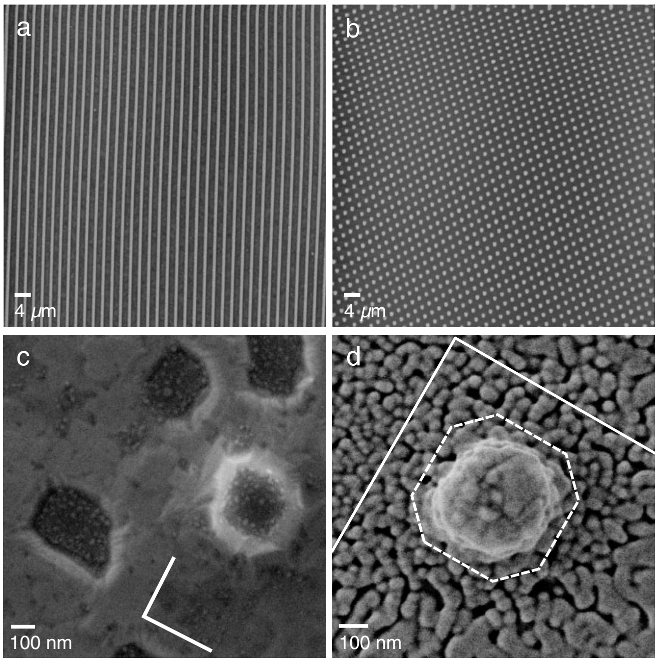

Figure 4. SEM images of line and columnar patterns of $PbTiO_3$ on a,b) silicon wafers and c,d) $SrTiO_3(001)$ obtained by micromolding a $PbTiO_3$ precursor solution. The width of the lines in (a) is ca. 700 nm, the diameter of the columns in (b) is ca. 1 µm, and their heights are 90 and 115 nm, respectively. The periodicities in (a) and (b) are 2.2 and 2 µm, respectively. The high-resolution SEM image in (c) shows a single column fabricated on $SrTiO_3$. Despite the somewhat rounded morphology of the $PbTiO_3$ crystal faces, the faceted nature of the column is clear with faces that are colinear with the holes in the thin, epitaxially grown film next to the column. The SEM image in (d) shows a somewhat larger column with faces that are collinear with the [100] and [010] edges of the underlying $SrTiO_3$ crystal, as indicated by the lines. The diameters of the columns are ca. 300 and 400 nm in (c) and (d), respectively. The images in (c) and (d) have been taken at the edge of the molded area, where the reproduction of the mold pattern has a somewhat lower fidelity, resulting in relatively smaller column diameters and an increased film thickness between the columns.

the epitaxial growth of the micromolded pattern requires diffraction from individual columns (such as in a transmission electron microscope), the symmetry observed in Figure 4c is strongly indicative of the epitaxial nature of this feature. Note that the perforated layer between the columns arises from incomplete micromolding. This can be significantly reduced by optimizing the micromolding process.

An interesting aspect of this experiment is the shrinkage observed during the pyrolysis of the films. For laterally continuous films, crack formation is not often observed (the film shown in Fig. 1a is an exception, and has been chosen for the contrast in the image). This implies that the continuous films shrink only normal to the surface. On the other hand, patterned films exhibit lateral shrinkage. This effect seems to be dependent on the material of the substrate and/or the deposited layer. It is more pronounced for Al_2O_3 and ZnO on glass, which have a lateral contraction that depends on the pattern geometry (ca. 80–90 %). $PbTiO_3$ on silicon wafers exhibits a much smaller lateral shrinkage of ca. 40–50 %. Evidently, the film material is more strongly pinned to the substrate throughout the processing of the film, thus suppressing the lateral shrinkage. As the overall volume contraction is ca. 95 % for the three systems, the maximum achievable aspect ratio (height-to-width ratio) of the oxide patterns depends on the amount of lateral shrinkage and the aspect ratio (feature-depth-to-width) of the mold.

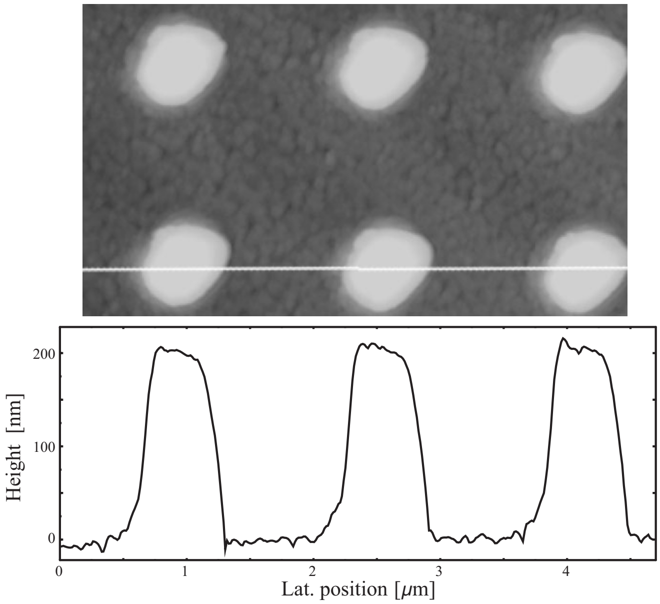

Figure 5. The AFM scan is a magnification of the sample shown in Fig. 4c and d. The ca. 600 nm wide and ca. 200 nm high columns, which are imaged close to the edge of the sample, are less-well formed than the 1 µm columns in the center of the sample. The lateral scale of the topography image is given by the cross section.

3. Conclusions

This article describes an extension of well-established soft-lithography techniques. By using a metal nitrate-containing precursor solution as a lithography resist, it is possible to create patterns of simple and complex oxide ceramics with lateral dimensions down to several hundreds of nanometers. Depending on the nature of the substrate, the obtained ceramic layers are amorphous, polycrystalline, or epitaxially oriented with respect to the underlying substrate. The recipe used is rather generic and we expect that a large number of different ceramics can be patterned by using this process. Together with the possibility of epitaxial alignment, this constitutes a promising strategy for the creation of functional nanostructures that were hitherto primarily accessible only through more complex and expensive experimental techniques. Using a simple rubber stamp, it should be possible to pattern ferromagnetic, ferroelectric, piezoelectric, and superconducting materials over large areas with high spatial definition.

While conceptually promising, our results also show the limitations of this specific soft-lithography method. The high-magnification images in Figure 4 clearly show that residual material remains between the lithographically replicated structures, potentially limiting the utility of this method. While in principle this could be remedied by post-processing the sample (such as by an etching step), the application of other soft-lithography methods will likely lead to better results. Very recent results indicate that electro-hydrodynamic lithography[19] and solvent-assisted embossing[20] do not suffer from these deleterious effects.

Our research demonstrates an approach for patterning inorganic materials using a soft-lithography method. Starting from a liquid precursor material, epitaxially grown sub-micrometer-scale patterns have been obtained.

4. Experimental

The nitrates used, $Al(NO_3)_3{\cdot}9\,H_2O$, $Zn(NO_3)_2{\cdot}6\,H_2O$, $Pb(NO_3)_2$, and $Ti(NO_3)_4$, were obtained from Aldrich. The solvent used was DMF, and the polymer used was PAA with a weight-average molecular weight (M_w) of 2 kg mol^{-1} (Aldrich). Similar results were also obtained using 2-methoxyethanol as the solvent or poly(methacrylic acid) as the polymer. The metal nitrates were first dissolved in DMF. In the case of $PbTiO_3$, $Pb(NO_3)_2$ and $Ti(NO_3)_4$ were dissolved in a 1:1 molar ratio. After dissolution of the nitrates, PAA was added. The weight ratio of metal nitrates to PAA was 1:1 for the Al_2O_3 and ZnO films and 1:1.5 for $PbTiO_3$. This resulted in clear, viscous solutions that were stable for many months.

The substrates used were microscope cover slips (SiO_2:B), polished wafers from Si(001) single crystals (covered by an amorphous oxide layer), and polished $SrTiO_3$(001) single-crystal plates (TBL-Kelpin, Germany). The substrate surfaces were cleaned in a jet of CO_2 crystals ("snow-jet" [21]), followed by plasma etching in an air plasma (5×10^{-4} Pa). For the silicon wafer, this resulted in a water contact angle of less than 2°.

Homogeneous films were made by spin-coating and patterned precursor films were made by micromolding. Relief-patterned molds of PDMS were obtained by using the Sylgard 184 kit (Dow Corning). After mixing and degassing the two-component mixture, it was cast onto a relief-patterned master (X'lith, Germany) consisting of a pattern that was etched into a silicon wafer (etching depth of ca. 950 nm). After curing overnight at 40 °C, the PDMS mold was removed from the master. Mold release was facilitated by coating the silicon master with a self-assembled monolayer of octadecyltrichlorosilane prior to PDMS casting. A drop of the precursor solution was placed onto the substrate and the PDMS mold was pressed into it. The sample and mold were placed on a hot stage set at 80 °C for 50 min to allow the solvent to diffuse into the mold. In one case (Fig. 2c and e), the precursor was spin-cast onto the substrate and the mold was pressed into the resulting viscous film.

After film fabrication, the sample was subjected to a high-temperature treatment to degrade the polymer (at ca. 500 °C), and to oxidize and crystallize the ceramic phase. The following heating protocol was used: from 80 to 200 °C at 10 °C min^{-1}, from 200 to 500 °C at 5 °C min^{-1}, from 500 °C to T_{max} at 10 °C min^{-1}, constant temperature T_{max} for 90 min, cooling from T_{max} to room temperature at ca. 10 °C min^{-1}. T_{max} was 630 °C for Al_2O_3 and ZnO and 700 °C for $PbTiO_3$. The heating was carried out in air. The appearance of the films depended on the details of this heating protocol. All films were imaged by using optical microscopy, AFM (Veeco Dimension 3100), and SEM (JEOL 6320F operated at 1.5 kV). The phase composition and out-of-plane alignment was determined by using X-ray ω–2θ scans taken on a two-circle diffractometer (Philips PW 1820, Cu Kα radiation). The in-plane epitaxial alignment was investigated by a ϕ–ψ scan (pole-figure) on a four-circle diffractometer (Philips X'pert MRD, Cu Kα radiation). Al_2O_3 films were also examined by using transmission electron microscopy (TEM, JEOL 2010F, operating at 200 kV) in diffraction mode. Al_2O_3-coated microscope cover slips were ground locally to zero thickness, yielding a large region with a sample thickness suitable for TEM analysis. The electron diffraction pattern was obtained as a function of the irradiation time.

Received: August 28, 2006
Revised: October 13, 2006

[1] Y. Xia, J. A. Rogers, K. E. Paul, G. M. Whitesides, *Chem. Rev.* **1999**, *99*, 1823.

[2] E. Kim, Y. Xia, G. M. Whitesides, *J. Am. Chem. Soc.* **1996**, *118*, 5722.

[3] M. Trau, N. Yao, E. Kim, Y. Xia, G. M. Whitesides, I. A. Aksay, *Nature* **1997**, *390*, 674.

[4] P. Yang, T. Deng, D. Zhao, P. Feng, D. Pine, B. F. Chmelka, G. M. Whitesides, G. D. Stucky, *Science* **1998**, *282*, 2244.

[5] N. L. Jeon, P. G. Clem, R. G. Nuzzo, D. A. Payne, *J. Mater. Res.* **1995**, *10*, 2996.

[6] W. S. Beh, Y. Xia, D. Qin, *J. Mater. Res.* **1999**, *14*, 3995.

[7] P. M. Moran, F. F. Lange, *Appl. Phys. Lett.* **1999**, *74*, 1332.

[8] S. Seraji, Y. Wu, N. E. Jewell-Larson, M. J. Forbess, S. J. Limmer, T. P. Chou, G. Cao, *Adv. Mater.* **2000**, *12*, 1421.

[9] U. P. Schönholzer, R. Hummel, L. J. Gauckler, *Adv. Mater.* **2000**, *12*, 1261.

[10] M. Heule, L. J. Gauckler, *Adv. Mater.* **2001**, *13*, 1790.

[11] H. Yang, P. Deschatelets, S. Brittain, G. M. Whitesides, G. D. Stucky, *Adv. Mater.* **2001**, *13*, 54.

[12] C. R. Martin, I. A. Aksay, *J. Phys. Chem. B* **2003**, *107*, 4261.

[13] J. S. Vartuli, M. Ozenbas, C.-M. Chun, M. Trau, I. A. Aksay, *J. Mater. Res.* **2003**, *18*, 1259.

[14] A. Seiffert, F. F. Lange, J. S. Speck, *J. Mater. Res.* **1995**, *10*, 680.

[15] F. F. Lange, *Science* **1996**, *273*, 903.

[16] O. F. Göbel, X. Du, T. Hibma, I. von Lampe, U. Steiner, *Eur. Phys. J. B* **2004**, *39*, 149.

[17] O. F. Göbel, X. Du, T. Hibma, I. von Lampe, F. Zygalski, U. Steiner, *Eur. Phys. J. B* **2005**, *42*, 483.

[18] J. H. Kim, F. F. Lange, C.-I. Cheou, *J. Mater. Res.* **1999**, *14*, 1194.

[19] N. E. Voicu, M. S. M. Saifullah, K. R. V. Subramanian, M. E. Welland, U. Steiner, *Soft Matter*, DOI: 10.1039/b616538a.

[20] N. E. Voicu, S. Ludwigs, E. J. W. Crossland, P. Andrew, U. Steiner, *Adv. Mater.*, DOI: 10.1002/adma.200601599.

[21] R. Sherman, D. Hirt, R. J. Vane, *J. Vac. Sci. Technol. A* **1994**, *12*, 1876.